




High-temperature superconducting nano-meanders made by ion irradiation

P Amari^{1,2}, C Feuillet-Palma^{1,2} , A Jouan^{1,2}, F Couëdo^{1,2}, N Bourlet^{1,2}, E Géron^{1,2}, M Malnou^{1,2}, L Méchin³, A Sharafiev^{1,2} , J Lesueur^{1,2}  and N Bergeal^{1,2}

¹ Laboratoire de Physique et d'Etude des Matériaux, ESPCI Paris, PSL Research University, CNRS, 10 Rue Vauquelin, F-75005 Paris, France

² Université Pierre and Marie-Curie, Sorbonne-Université, F-75005 Paris, France

³ Normandie Univ, UNICAEN, ENSICAEN, CNRS, GREYC, F-14000 Caen, France

E-mail: cheryl.palma@espci.fr

Received 18 July 2017, revised 31 October 2017

Accepted for publication 6 November 2017

Published 8 December 2017



Abstract

In this article, we report on the fabrication of very long $\text{YBa}_2\text{Cu}_3\text{O}_7$ nanowires in a meander shape patterned in a CeO_2 -capped thin film by high-energy oxygen ion irradiation. DC and RF characterizations outline the good superconducting properties of the nanowires whose geometry approaches the one used in single photon detectors. Their inductance, which mainly sets the maximum speed of these devices, has been measured on a wide range of temperature by mean of a resonant method. The extracted values are in agreement with the ones calculated from the geometry of the meanders and from the known London penetration depth in $\text{YBa}_2\text{Cu}_3\text{O}_7$ thin films.

Keywords: superconductor, YBCO, single photon detector, SSPD

(Some figures may appear in colour only in the online journal)

1. Introduction

Optical quantum information technologies (such as quantum key distribution), low-light level depth imaging, space-to-ground communications, atmospheric remote sensing are some examples of cutting edge technologies that require high efficiency infrared detectors with an ultimate sensitivity down to the single photon level as well as a very good time resolution [1]. The first proof-of-concept of a single photon detection mechanism occurring when a photon is absorbed by a superconducting nanowire biased close to its critical current has generated a real excitement in the community over the last decade [2]. Long, narrow and thin superconducting meanders inserted in a read-out line are the basic building blocks of this new kind of detectors called superconducting single photon detectors (SSPD). Considerable efforts have been put forth to improve significantly their performances until overcoming in many ways their semi-conductors based counterparts [3]. SSPD are nowadays commercially available, based on conventional low T_c materials such as NbN, NbTi or WSi.

Despite tremendous advantages offered by those detectors such as high quantum efficiency ($\sim 93\%$ at around $\lambda \sim 1.54 \mu\text{m}$) [4], high operating frequency ($\sim 1 \text{ GHz}$ [5]), low intrinsic dark count rate ($\sim 0.1 \text{ cps}$ [6]), low jitter ($\sim 18 \text{ ps}$ full width at half maximum [7]) and broad spectral range (from visible to mid-infrared $\lambda \sim 10.6 \mu\text{m}$ [8, 9]), the operating temperature well below 4 K for optimal performances prevents large scale applications. The fabrication of SSPD with high-temperature superconductors (HTS) such as $\text{YBa}_2\text{Cu}_3\text{O}_7$ would then provide two main benefits: the ability of working at higher temperature with simplified cryogenics, and the possibility of operating at higher frequency thanks to very short relaxation times [10]. However, $\text{YBa}_2\text{Cu}_3\text{O}_7$ implementation faces the main difficulty of preserving pristine superconducting properties during the nano-patterning process, because of defects creation or oxygen out-diffusion. Indeed, a typical NbN based SSPD has a thickness of 5 nm or lower, a width of 100 nm, and a total length of hundreds of microns. To maximize the perturbation induced by the photon absorption namely the hotspot [2], width and thickness must be at the nanometric scale. The signature of a self-stabilizing

hotspot relies on the hysteresis of the I - V curves as shown by Skocpol *et al* [11] and very recently by Arpaia *et al* [12] in short $\text{YBa}_2\text{Cu}_3\text{O}_7$ bridges. On the other hand, the length of the meander allows maximizing the absorption area of the detector. For a typical detector area of $100 \mu\text{m}^2$, a 100 nm wide meander has to be $500 \mu\text{m}$ long to optimize to detection surface efficiency. Structuring $\text{YBa}_2\text{Cu}_3\text{O}_7$ into this shape without modifying the bulk like superconducting properties represents therefore a main challenge. First attempts have been made using focused ion beam [13, 14]. Recently Arpaia *et al* used Ar ion beam etching (IBE) with protecting layers to pattern devices such as nano-SQUIDS with good properties [15]. They reported on the fabrication of $\text{YBa}_2\text{Cu}_3\text{O}_7/\text{La}_{0.7}\text{Sr}_{0.3}\text{MnO}_3$ [16] and $\text{YBa}_2\text{Cu}_3\text{O}_7$ [17] tens of microns long nanowires with a $100 \times 50 \text{ nm}^2$ cross-section and $\text{YBa}_2\text{Cu}_3\text{O}_7/\text{Au}$ [18] hundred of nanometers long ones with a cross-section down to $50 \times 50 \text{ nm}^2$, with a detection surface up to $5 \mu\text{m}^2$, while preserving superconducting properties. Photoresponse has been evidenced in some of these devices, but not at the single photon level. The longest nanowire in a meander shape ($430 \mu\text{m}$ long) was $1 \mu\text{m}$ wide in a 12 nm thick film, with a detection surface of $430 \mu\text{m}^2$. Small degradations were observed, as the critical temperature was lowered down to $\sim 70 \text{ K}$ [19]. However, no report of long and narrower meander on $\text{YBa}_2\text{Cu}_3\text{O}_7$ thin films has been made up to now.

In this work, we present the realization and the characterization of hundreds of microns long nano-meanders designed in 30 nm thick $\text{YBa}_2\text{Cu}_3\text{O}_7$ thin films. Their widths range from 100 to 750 nm and the corresponding detection surfaces from 562 to $45 \mu\text{m}^2$. We measured both the DC and microwaves properties of the devices which are found to be in good agreement with theoretical predictions. In particular, the inductance L of the devices, a key parameter that governs the reset time L/R_L of an SSPD (R_L is the load resistance of the circuit), has been extracted. Its value and its temperature dependence given by the London penetration depth one, agree very well with the expected ones in $\text{YBa}_2\text{Cu}_3\text{O}_7$.

2. Experiment

The manufacturing method used here relies on the high sensitivity to disorder of the d-wave superconducting order parameter of HTS. Irradiation with high-energy oxygen ions accelerated under a few tens of kV, generates punctual defects in the crystal structure that increase the normal resistivity and reduce T_c . A superconducting-insulating transition can be induced by increasing the defect density beyond a threshold. Superconducting devices can be designed by irradiating a $\text{YBa}_2\text{Cu}_3\text{O}_7$ thin film through a thick resist template patterned either by optical or e-beam lithography [20–24]. The exposed areas become insulating while the areas protected by the resist remain superconducting. The method was successfully applied to design Josephson TeraHertz heterodyne detectors [25–27]

and superconducting quantum interference filters [28] made from $\text{YBa}_2\text{Cu}_3\text{O}_7$ commercial Ceraco thin films [29].

For this study, we used 30 nm thick $\text{YBa}_2\text{Cu}_3\text{O}_7$ commercial thin films grown on a sapphire substrate and capped with a 8 nm thick CeO_2 layer, processed as follows. A 200 nm thick gold 50Ω coplanar waveguide (CPW) transmission line is first deposited on top of the CeO_2 -capped $\text{YBa}_2\text{Cu}_3\text{O}_7$ thin film using conventional lift-off technique. In this step, the CeO_2 layer is removed by a 500 eV Ar^+ IBE prior to the gold deposition in order to ensure a good electrical contact with the $\text{YBa}_2\text{Cu}_3\text{O}_7$ layer. In a second step, a negative ma-N resist is coated on top of the sample and the meander is patterned by e-beam lithography between the central line and the ground of the CPW (figure 1(a)). Finally, a 30 keV oxygen ion irradiation at a dose of $5 \times 10^{14} \text{ at cm}^{-2}$ is performed to define the nano-meander into the $\text{YBa}_2\text{Cu}_3\text{O}_7$ layer. During this step, all the areas of the sample, which are not protected either by the resist (meander) or by the gold layer (CPW), become insulating.

The main advantage of this method is that the HTS nanowire is totally encapsulated between the insulating $\text{YBa}_2\text{Cu}_3\text{O}_7$ film on the side and the CeO_2 layer on the top, preventing oxygen loss. The energy and the fluence of oxygen ions necessary to make $\text{YBa}_2\text{Cu}_3\text{O}_7$ insulating without altering the nanowire have been optimized through numerical simulation using the Monte Carlo based code TRIM [30]. This is illustrated for the 100 nm wide meander in figure 1(f), by a colour-plot of the calculated local displacement per atoms (dpa) which quantifies the defect density. For dpa $> 10\%$, the material is insulating (white line).

In this paper, we report specifically on three nano-meanders whose dimensions are $750 \text{ nm} \times 750 \mu\text{m}$, $200 \text{ nm} \times 450 \mu\text{m}$ and $100 \text{ nm} \times 450 \mu\text{m}$ respectively, folded into a meander shape (figure 1(d)). We checked that the actual widths of the conducting channels correspond to the nominal ones through atomic force microscopy imaging (figures 1(b)–(e)), thanks to a tiny swelling of the layer under irradiation ($\sim 2 \text{ nm}$ in height). The origin of such a swelling, already reported in the literature [31], is not fully established yet: it is likely related to partial amorphization of the film/substrate system. The sample are connected via a PC-board, and mounted onto a cold sample holder in a cryogen-free cryostat. The DC resistance versus temperature (R - T) and the current versus voltage (I - V) curves are recorded through four probes measurements. RF measurements are performed through semi-rigid co-axial wires.

3. Results

Resistance versus temperature curves of the nano-meanders are reported in figure 2(a). The 750 nm wide nanowire has a midpoint critical temperature T_c of 86.7 K (defined as a 50% resistance drop), identical to the one of the unprocessed film. T_c decreases down to 86.2 K and 85.8 K for the 200 nm and the 100 nm wide ones respectively. The I - V characteristics of the 100 nm wide nanowire is presented in figure 2(b) for

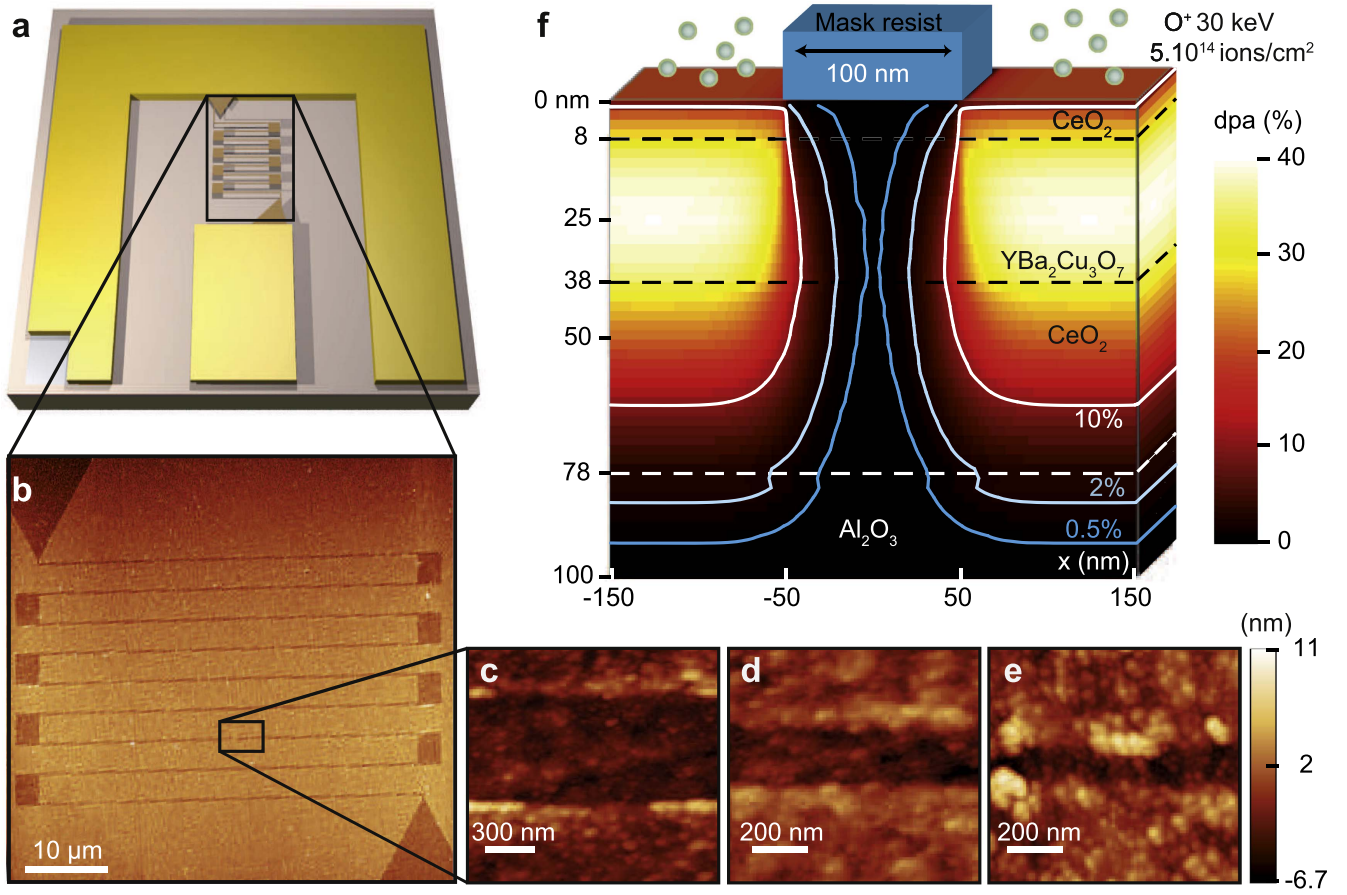


Figure 1. (a) Scheme of a typical sample consisting in a nano-meander embedded into a gold CPW. (b)–(e) AFM topography images of conducting channels defined by ion irradiation (see text for an explanation of the contrast). (b) The whole meander, (c) focus on a 750 nm wide wire, (d) 200 nm and (e) 100 nm wide one. Note that white parts are negative ma-N resist residues. (f) TRIM numerical simulation profile of the ion irradiation damages in unity of displacement per atom (dpa) produced by a 30 keV oxygen ion irradiation (dose of $\Phi = 5 \times 10^{14}$ ions cm^{-2}) for a 100 nm wide nanowire protected by a ma-N resist. Contour lines corresponding to 0.5%, 2% and 10% dpa (insulating limit) are also indicated.

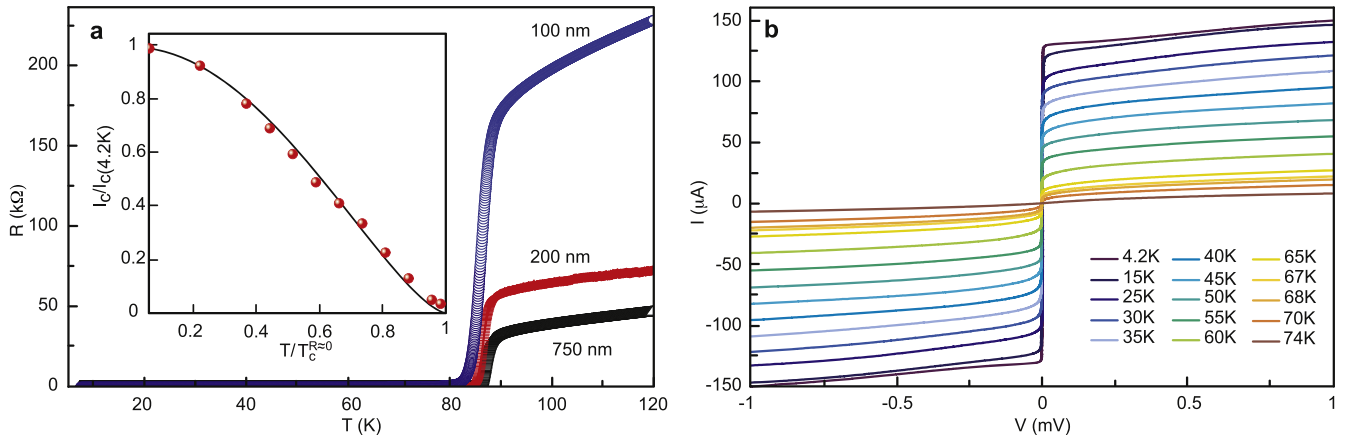


Figure 2. (a) Resistance as a function of temperature for $\text{CeO}_2/\text{YBa}_2\text{Cu}_3\text{O}_7$ /nano-meanders of different widths—100 nm (blue circle), 200 nm (red), 750 nm (black). Inset: corresponding dependence of the critical current with temperature. The black line is a fit with the Bardeen formula (see text). (b) Current–voltage characteristics of a 100 nm wide nanowire at different temperatures.

temperatures ranging from 4.2 to 74 K. They are typical of a flux-flow regime as already observed by other authors [12, 32]. At the lowest temperature, the transition to the resistive state as the current is slightly increased above the critical current I_c is abrupt, but no hysteresis is observed.

The critical current density of the 100 nm nanowire is $4.3 \times 10^6 \text{ A cm}^{-2}$ at 4.2 K. This value is comparable to the ones reported for $\text{YBa}_2\text{Cu}_3\text{O}_7$ nanowires [17, 32, 33], and is approximately two orders of magnitude smaller than the depairing limit $j_d \sim 5 \times 10^8 \text{ A cm}^{-2}$. Its temperature

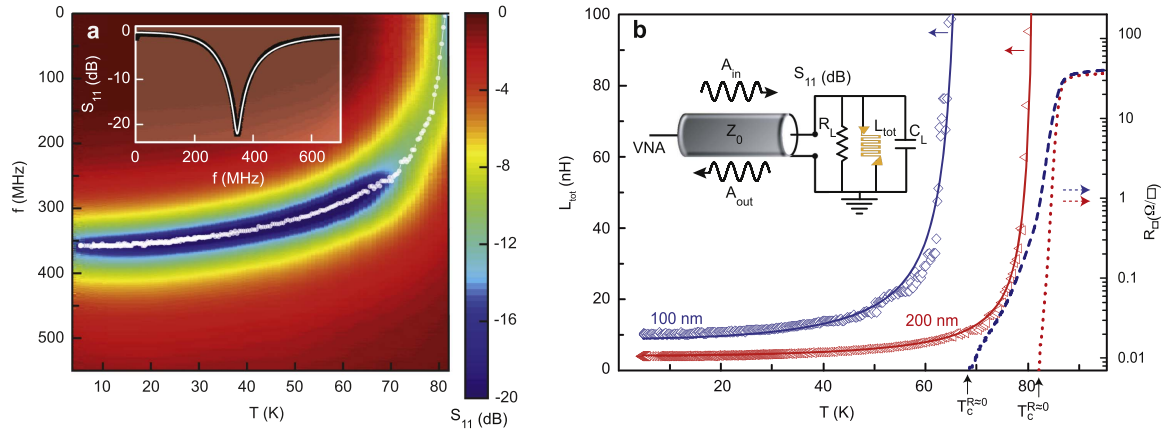


Figure 3. (a) Colour-plot of S_{11} as a function of frequency and temperature for the 200 nm wide meander showing the shift of resonant frequency f_0 with temperature. Inset (a): S_{11} in dB at $T = 30$ K for the 200 nm wide meander (black line). The white solid line corresponds to the fit of S_{11} using the expression (1). (b) Temperature dependence of L_{tot} for the meanders: 100 nm wide (blue diamonds $T_c^{R=0} = 68$ K), 200 nm (red triangles $T_c^{R=0} = 82$ K), and the corresponding fits in continuous lines. Inset (b): schematic view of the resonant circuit.

dependence follows the Ginzburg–Landau expression generalized by Bardeen for dirty superconductors [34] over the whole range in temperature (inset 2(a)): $I_c(T)/I_c(4.2 \text{ K}) = (1 - (T/T_c^{R=0})^2)^{-3/2}$ with $T_c^{R=0} = 68$ K. Here we notice a difference between $T_c^{R=0}$ and the midpoint critical temperature T_c defined previously in figure 1. From the log-scale plot of R – T curves in figure 3(b), $T_c^{R=0}$ corresponds to the critical temperature for the zero resistance state, taking the usual criteria of an electric field of $0.5 \mu\text{V cm}^{-1}$ within the sample equivalent to a resistance per square of $R_{\square} \sim 5.10^{-3} \Omega/\square$. The presence of a foot of small amplitude ($<0.1 \Omega/\square$) in the resistive transition of the 100 nm wide wire (figure 3(b)) indicates that a short part of the $450 \mu\text{m}$ long nanowire has not optimum properties. This cannot be explained by the sole irradiation process. Indeed, TRIM calculation of the defect density, as displayed in figure 1(f), shows that ions penetrate under the protected area over a mean distance of 25 nm in our irradiation conditions, and produce a small amount of defects. We can calculate the local T_c through the Abrikosov–Gorkov depairing law $T_c(\text{dpa})$ that holds in disordered $\text{YBa}_2\text{Cu}_3\text{O}_7$ [23, 35]. The light (respectively dark) blue line in figure 1(f) corresponds to a 2% (respectively 0.5%) dpa, that is a 30% (respectively 10%) T_c reduction. The lowest local T_c of the 30 nm thick nanowire is therefore expected to be around 78 K (90% of the pristine film $T_c^{\text{max}} = 86.7$ K), much higher than 68 K, the measured $T_c^{R=0}$. Moreover, T_c is higher towards the surface, and the simulation shows that a ~ 50 nm wide channel just beneath the photoresist should have a T_c close to the maximum one. This is what is observed since the midpoint T_c is 85.6 K (98% of T_c^{max}) for the 100 nm wide meander line, and 86.2 K (99% of T_c^{max}) for the 200 nm wide one. We conclude from this study that the resistive foot that develops corresponds to a localized zone with a lower T_c , either because the pristine film was not completely homogeneous, either because of degradation during the fabrication process. It is worth mentioning that the devices have been thermally cycled up to room temperature and measured several times within a maximum period of 30 months. While the

midpoint T_c stays exactly the same for all of them, the resistive foot develops during the first months and then stays the same (for the 100 nm wide meander, $T_c^{R=0}$ saturates at 65 K). This behaviour indicates that non-optimum zones do change slightly upon cycling and ageing, while the main part of the meander is stable.

A detected event in a SSPD, i.e. a photon absorbed by the device, generates a voltage pulse whose characteristic time is dominated by the ratio L/R_L , where L is the inductance and R_L the load resistance of the circuit. We designed a set-up to measure the inductance of the meanders in the low GHz frequency range. In a microwave circuit, the reflection coefficient S_{11} at a discontinuity between a transmission line and a load circuit is given by: $S_{11} = (Z_L - Z_0)/(Z_L + Z_0)$, where $Z_0 = 50 \Omega$ is the characteristic impedance of the transmission line and Z_L is the load impedance. In this experiment, a lumped element resonant circuit involving the nano-meander is directly connected to the CPW line (inset figure 3(b)), and the reflection coefficient S_{11} is measured using a vector network analyser. The device is connected in parallel with a 24 pF surface mounted device (SMD) capacitor C_L and a SMD resistor $R_L \simeq 50 \Omega$, both located close to the nanowire to minimize parasitic inductances and capacitances. The nanowire acts as the inductor of a parallel RLC circuit whose impedance is:

$$Z_L = \frac{1}{\frac{1}{R_L} + \frac{1}{jL\omega} + jC_L\omega}. \quad (1)$$

The total inductance $L = L_K + L_G + L_p$ is the sum of a geometric term L_G , a kinetic term L_K due to the inertia of Cooper pairs in the superconducting state, and a parasitic inductance L_p . At the resonant frequency, the circuit impedance is purely real and $Z_L \simeq R_L \simeq 50 \Omega$. The microwave power is dissipated in the load circuit and a dip is observed in the magnitude of $|S_{11}|$ along with a 2π phase shift. Figure 3(a) shows a colour-plot of S_{11} as a function of frequency and temperature for the 200 nm wide meander. An absorption dip is evidenced (down to -20 dB), at a resonant frequency $f_0 = 1/\sqrt{LC}$ which strongly decreases with temperature. We

fitted the data for each temperature (see for instance the 30 K trace in the inset figure 3(a)) using $C_L = 24$ pF. We therefore retrieve the inductance $L(T)$ which includes both the temperature dependent L_{tot} and the constant L_p .

The geometric inductance for a wire of length $l(\text{mm})$, width $w(\text{mm})$ and thickness $e(\text{mm})$ is $L_G = 0.2 \cdot l (0.5 + (w + e)/3l + \ln(2 \cdot l/(w + e))) (\text{nH})$ [36], while the kinetic one is $L_K = \mu_0 \lambda(T)^2 \cdot (l/we)$, where λ is the London penetration depth of the superconductor. Within the two fluids model, and according to the Gorter Casimir expression, its temperature dependence is: $\lambda(T)^2 = \lambda_0^2 / (1 - (T/T_c)^\alpha)$ where λ_0 is the zero-temperature penetration depth, T_c the critical temperature and α a parameter whose value has been found to be 2 in cuprates [28, 33, 37, 38].

In figure 3(b), we plot L_{tot} (symbols), determined from the resonance frequency, as a function of temperature for the 100 and 200 nm wide nanowires. We also show the best fits (solid lines) assuming $L_{\text{tot}} = L_G + L_K$ and fixing T_c as $T_c^{R \approx 0}$ according to DC measurements (see above), together with $\alpha = 2$. The only free parameter is therefore λ_0 which is found to be 200 ± 8 nm and 186 ± 8 nm for the 100 nm and 200 nm wide wires respectively. These values are in very good agreement with previously reported ones in the literature [33, 38].

4. Discussion

The above presented results show that ion irradiation is a suitable technique to make long and thin $\text{YBa}_2\text{Cu}_3\text{O}_7$ nanowires. The smallest cross-section area that we made is $30 \times 100 \text{ nm}^2$, and compares favourably with the best results in the literature. Superconducting properties are preserved up to 68 K for the smallest nanowires (100 nm wide). RF data and the fit that we provide show that the whole $450 \mu\text{m}$ long nanowire participates to the kinetic inductance of the device, which is important in the perspective of making SSPD out of ion-irradiated $\text{YBa}_2\text{Cu}_3\text{O}_7$ nanowires. Indeed, SSPD operation requires two important points. The first one is the ability of detecting a single photon absorption through the formation of a hot-spot in the wire [11]. The second one is to have a sizeable interaction cross-section of the device, in order to reach the highest possible quantum efficiency, and to detect all the photons that come onto the SSPD. This requires to maximize the effective interaction area of the meander, and for photons in the IR and far-IR range that are targeted, to make typically a $10 \mu\text{m}$ large square with a filling factor 50% [1]. For a 100 nm wide wire that corresponds approximately to a $500 \mu\text{m}$ long meander, a geometry close to the nanowires we have discussed here. Let us now discuss the first requirement to make a SSPD. As shown by Skocpol *et al* [11], the propagation of the local heating created by the photon in the hotspot to the whole meander is related to a hysteretic I - V characteristics of the wire. Therefore, devices with such I - V curves are good candidates to make SSPD, and ours do not belong to this category. Until very recently, that was the case

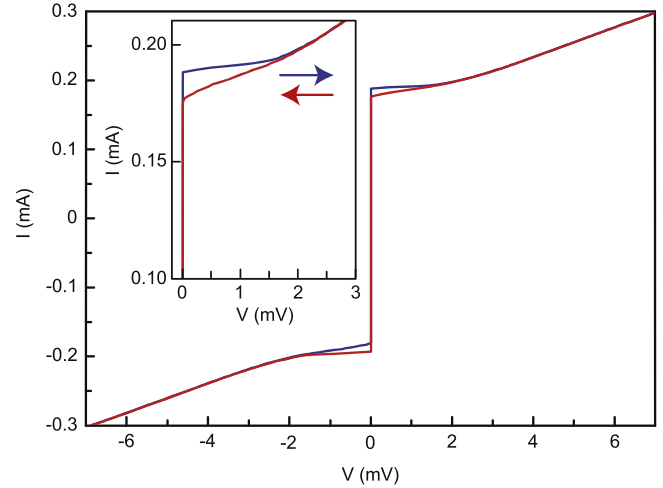


Figure 4. Hysteretic current–voltage characteristic of a 100 nm wide, 20 μm long and 30 nm thick nanowire at 5 K. The value of the differential resistance is $dV/dI \sim 55 \Omega$, which corresponds to approximately 1% of the normal resistance at 100 K.

for all HTSc based nanowires reported in the literature [17, 18, 32]. In their recent paper, Arpaia *et al* [12] present data on very short nanowires (typical size 10 nm thick, 100 nm wide and 100–500 nm long), which do display a hysteretic behaviour at low temperature. Interestingly, they report that wires with a critical current density lower than $J_c \sim 5 \times 10^6 \text{ A cm}^{-2}$ show flux-flow I - V curves, while those with higher J_c show hysteretic ones. The current density of the 100 nm wire presented here ($J_c \sim 4.3 \times 10^6 \text{ A cm}^{-2}$) is just below this threshold, and does show a flux-flow behaviour. We recently made shorter nanowires (20 μm long) with the same cross-section than the ones reported here. Their critical current density is higher than $5 \times 10^6 \text{ A cm}^{-2}$, namely $7 \times 10^6 \text{ A cm}^{-2}$ for the one presented in figure 4. As can be seen, I - V characteristic is hysteretic at 5 K. The voltage swing is on the order of 2 mV as in Arpaia *et al*'s article [12]. This is a first report that needs to be explored in more detail, but which proves that making $\text{YBa}_2\text{Cu}_3\text{O}_7$ nanowires by ion irradiation is a possible route towards HTSc SSPD. The goal is now to make nanowires with both an extended area and a hysteretic I - V characteristic. Working with thinner films (typically 10 nm) would be a first improvement. In that case, both ion-irradiation energy and ions fluence have to be optimized. An alternative way will be explored, to further reduce the cross-section of the nanowire. The recent development of 30 keV He focused ion beam machines has been successfully used to fabricate $\text{YBa}_2\text{Cu}_3\text{O}_7$ Josephson junctions by direct writing in a thin layer. We can use it to draw the meander by locally irradiating the zones to be made insulating with a very high precision [39]. Indeed, because of the light He mass, the lateral straggling at 0.5% dpa is around 20 nm whereas in our method using oxygen ion, it is 50 nm for the same amount of defects. Then we hope to decrease further the width of the nanowires.

5. Conclusion

In conclusion, we have presented a new reliable method to make $\text{YBa}_2\text{Cu}_3\text{O}_7$ nanowires in a meander shape, based on high-energy ion irradiation. Good superconducting characteristics are preserved for devices as narrow as 100 nm wide, over lengths up to 450 μm . Protected by a top CeO_2 layer and embedded in an insulating $\text{YBa}_2\text{Cu}_3\text{O}_7$ matrix, the nanowires are robust and sustain thermal cycling. Using a resonant method, we have accurately measured their temperature dependent inductance—a key parameter for high-speed operation—which agrees with the expected one for the whole nanowire. This is a first step towards the realization of photo-sensitive devices with a large detection efficiency. We also report on a preliminary result which shows that shorter nanowires may display a hysteretic behaviour, a key requirement for single photon detection.

Acknowledgments

The authors thank Yann Legall for ion irradiations, Jean-Claude Villégier and M Rosticher for fruitful discussions, T Ditchi and J Lucas for RF experiments support. This work has been supported by the french agencies ANR and DGA, by the Region Ile-de-France in the framework of DIM Nano-K and by the European Community (NQO COST Action).

ORCID iDs

C Feuillet-Palma  <https://orcid.org/0000-0002-8389-5756>

A Sharafiev  <https://orcid.org/0000-0002-8780-9261>

J Lesueur  <https://orcid.org/0000-0002-5843-187X>

References

- [1] Natarajan C M, Tanner M G and Hadfield R H 2012 *Supercond. Sci. Technol.* **25** 063001
- [2] Gol'tsman G N, Okunev O, Chulkova G, Lipatov A, Semenov A, Smirnov K, Voronov B, Dzardanov A, Williams C and Sobolewski R 2001 *Appl. Phys. Lett.* **79** 705
- [3] Hadfield R H 2009 *Nat. Photon.* **3** 696
- [4] Marsili F et al 2013 *Nat. Photon.* **7** 210
- [5] Rosfjord K M, Yang J K W, Dauler E A, Kerman A J, Anant V, Voronov B M, Goltsman G N and Berggren K K 2006 *Opt. Express* **14** 527
- [6] Shibata H, Shimizu K, Takesue H and Tokura Y 2013 *Appl. Phys. Express* **6** 072801
- [7] You L et al 2013 *AIP Adv.* **3** 072135
- [8] Marsili F, Bellei F, Najafi F, Dane A E, Dauler E A, Molnar R J and Berggren K K 2012 *Nano Lett.* **12** 4799
- [9] Korneev A, Korneeva Y, Florya I, Voronov B and Goltsman G 2012 *Phys. Proc.* **36** 72
- [10] Lindgren M, Currie M, Williams C, Hsiang T Y, Fauchet P M, Sobolewski R, Moffat S H, Hughes R A, Preston J S and Hegmann F A 1999 *Appl. Phys. Lett.* **74** 853
- [11] Skocpol W J, Beasley M R and Tinkham M 1974 *J. Appl. Phys.* **45** 4054
- [12] Arpaia R, Golubev D, Baghdadi R, Ciancio R, Dražić G, Orgiani P, Montemurro D, Bauch T and Lombardi F 2017 *Phys. Rev. B* **96** 1
- [13] Booiij W E, Pauza A J, Tarte E J, Moore D F and Blamire M G 1997 *Phys. Rev. B* **455** 14600
- [14] Lee S G, Oh S-H, Kang C S and Kim S-J 2007 *Physica C* **460–462** 1468
- [15] Arpaia R, Arzeo M, Baghdadi R, Trbaldo E, Lombardi F and Bauch T 2016 *Supercond. Sci. Technol.* **30** 014008
- [16] Arpaia R, Ejrnaes M, Parlato L, Cristiano R, Arzeo M, Bauch T, Nawaz S, Tafuri F, Pepe G P and Lombardi F 2014 *Supercond. Sci. Technol.* **27** 044027
- [17] Arpaia R, Ejrnaes M, Parlato L, Tafuri F, Cristiano R, Golubev D, Sobolewski R, Lombardi F and Pepe G P 2015 *Physica C* **509** 16
- [18] Arpaia R, Nawaz S, Lombardi F and Bauch T 2013 *IEEE Trans. Appl. Supercond.* **23** 1101505
- [19] Curtz N, Koller E, Zbinden H, Decroux M, Antognazza L, Fischer Ø and Gisin N 2010 *Supercond. Sci. Technol.* **23** 045015
- [20] Chen K, Cybart S and Dynes R 2004 *Appl. Phys. Lett.* **85** 2863
- [21] Bergeal N, Grison X, Lesueur J, Faini G, Aprili M and Contour J P 2005 *Appl. Phys. Lett.* **87** 102502
- [22] Cybart S A, Chen K, Cui Y, Li Q, Xi X X and Dynes R C 2006 *Appl. Phys. Lett.* **88** 012509
- [23] Bergeal N, Lesueur J, Sirena M, Faini G, Aprili M, Contour J-P and Leridon B 2007 *J. Appl. Phys.* **102** 083903
- [24] Cybart S, Anton S, Wu S, Clarke J and Dynes R 2009 *Nano Lett.* **9** 3581
- [25] Malnou M, Feuillet-Palma C, Ulysse C, Faini G, Febvre P, Sirena M, Olanier L, Lesueur J and Bergeal N 2014 *J. Appl. Phys.* **116** 074505
- [26] Malnou M et al 2012 *Appl. Phys. Lett.* **101** 233505
- [27] Sharafiev A, Malnou M, Feuillet-Palma C, Ulysse C, Febvre P, Lesueur J and Bergeal N 2016 *Supercond. Sci. Technol.* **29** 074001
- [28] Ouanani S, Kermorvant J, Ulysse C, Malnou M, Lematre Y, Marcilhac B, Feuillet-Palma C, Bergeal N, Crt D and Lesueur J 2016 *Supercond. Sci. Technol.* **29** 094002
- [29] <http://ceraco.de/>
- [30] Ziegler J F and Biersack J P 2004 *SRIM* (New York: IBM)
- [31] Hurand S et al 2016 *Appl. Phys. Lett.* **108** 052602
- [32] Nawaz S, Bauch T and Lombardi F 2011 *IEEE Trans. Appl. Supercond.* **21** 164
- [33] Rauch W, Gornik E, Slkner G, Valenzuela A A, Fox F and Behner H 1993 *J. Appl. Phys.* **73** 1866
- [34] Bardeen J 1962 *Rev. Mod. Phys.* **34** 667
- [35] Trastoy J, Malnou M, Ulysse C, Bernard R, Bergeal N, Faini G, Lesueur J, Briatico J and Villegas J E 2014 *Nat. Nanotechnol.* **9** 710715
- [36] Yue C P and Wong S S 2000 *IEEE Trans. Electron Devices* **47** 560
- [37] Johansson J, Cedergren K, Bauch T and Lombardi F 2009 *Phys. Rev. B* **79** 214513
- [38] Wolf T, Bergeal N, Lesueur J, Fourie C, Faini G, Ulysse C and Febvre P 2013 *IEEE Trans. Appl. Supercond.* **23** 1101205
- [39] Cybart S A, Cho E Y, Wong T J, Wehlin B H, Ma M K, Huynh C and Dynes R C 2015 *Nat. Nanotechnol.* **10** 598–602